

Duplex NiP/NiMo-(h)BN Co-Electroplating: Evaluation of Nanohardness, Room and High Temperature Wear Behaviors

Mert Aydın¹, Hasan Algül^{2*}, Figen Algül³, Sezer Tan⁴, Ahmet Alp⁵

Sakarya University, Faculty of Engineering, Department of Metallurgical and Materials Science, Sakarya, Türkiye, mrtaaydin@gmail.com, halgul@sakarya.edu.tr, figenozboz@gmail.com, sezertan@sakarya.edu.tr, alp@sakarya.edu.tr
*Corresponding Author

ARTICLE INFO

ABSTRACT

Keywords:

Electrodeposition
Pulse reverse current
(h)BN Reinforcement
Duplex coating
Nanohardness
High temperature wear

Article History:

Received: 01.11.2024
Revised: 18.12.2024
Accepted: 29.01.2025
Online Available: 13.02.2024

This study explores the fabrication of duplex NiP/NiMo-(h)BN co-electrodeposits on steel substrates utilizing the reverse pulsed current (RPC) deposition method. Duplex electrodeposition offers superior physical and mechanical properties compared to single-layer plating, rendering it highly suitable for applications demanding enhanced wear resistance and adhesion. Here, NiP was selected as the inner layer due to its strong adhesion to steel, while NiMo-(h)BN served as the outer layer to maximize wear resistance. Both NiP and NiP/NiMo-(h)BN electrodeposits were deposited using a reverse pulsed current approach to enhance high temperature wear resistance of the steel substrate. The incorporation of (h)BN nanosheets into the NiMo matrix markedly enhanced the nano-hardness of the deposit, increasing it from 4.26 GPa to 5.23 GPa with the incorporation of 10 g/L (h)BN. Additionally, the solid lubrication properties of (h)BN reduced the friction coefficient of the duplex electrodeposit from 0.7 to 0.4 μ . At 400 °C, the duplex NiP/NiMo-(h)BN co-electrodeposit exhibited a wear rate of 1.77×10^5 mm³/Nm, nearly doubling the wear resistance of the duplex NiP/NiMo alloy deposit.

1. Introduction

Many techniques are used in the production of pure metals and alloys. The most widely recognized and utilized techniques for producing composites and alloys include direct current (DC), pulse current (PC), and pulse-reverse current (PRC) methods. [1, 2].

The most preferred coating type in the production of pure metals, alloys and composite coatings is DC electrodeposition [3]. It provides a wide and easy area of use due to its high physical and chemical properties, reaching high coating thickness quickly. However, irregular and inhomogeneous deposit thicknesses are the disadvantages of the method. Pulse current (PC) and pulse-reverse current (PRC) are a well-known method widely used in the field of alloy and composite deposition. When used instead of direct current, pulse electroplating provides

better adhesion strength to the substrate as well as more uniform deposit thickness. It also has several advantages, including improved mechanical properties [4].

Among the transition metal alloys, NiP deposits have attracted much attention due to their functional properties [5, 6]. NiP deposits have attracted much attention due to their good corrosion and wear properties, high hardness, excellent workability and good adhesion strength. NiP deposits are widely used in technological applications, in micro galvanic applications as catalytic coatings for hydrogen evolution reactions, in the automotive industry and in decorative applications [7].

Alloys containing Mo (molybdenum) are highly preferred coating types due to superior hardness, wear, thermal and corrosion resistance. NiMo deposits offer an important alternative to harmful

chrome, especially in the aviation industry [8]. Molybdenum cannot be deposited alone in its pure form [9]. Therefore, it is typically electrodeposition with another iron group metal such as iron, nickel or cobalt by co-deposition [10]. Alloy coatings cannot achieve high hardness, mechanical and tribological properties alone, and in this case, composite deposits can be preferred, and higher deposit performances can be achieved.

Hexagonal boron nitride, BN(h) ceramic particles are a popular reinforcement phase used to obtain composite coatings. BN(h) is preferred due to its chemical inertness, low thermal expansion coefficient, low dielectric constant, good thermal shock resistance, lubricity and high thermal properties [11].

In recent years, metal matrix composite (MMC) deposition have been obtained by reinforcing polymer and ceramic particles into the metal matrix. Composite depositions increase the mechanical, tribological and hardness properties of the metal matrix to very high levels, allowing the deposits to provide high performance even in different environments. In this way, it ensures that the deposits provide high performance at higher operating temperatures [12]. Composite deposition can be produced as a single layer or as duplex.

Duplex depositions leverage the combined structural attributes of two distinct layers, utilizing their synergistic interaction to address potential limitations found in single-layer coatings [13]. Studies have shown that duplex deposits offer superior wear resistance compared to single-layer systems and present the advantage of customizable inner and outer layer combinations. This adaptability enables optimization of coating performance based on specific requirements [13–15].

NiMo-(h)BN composite deposits emerge as next-generation materials providing exceptional wear resistance under high-temperature conditions. These deposits are applied to the surface by the electrodeposition method and combine the hardness and temperature resistance of Ni and Mo with the self-lubricating properties of (h)BN. Thus, friction and wear on surfaces operating at

high temperatures are significantly reduced and material life is extended.

This study aims to evaluate the wear resistance and performance characteristics of duplex NiP/NiMo-(h)BN co-electrodeposits designed for high-temperature applications. Within the scope of the study, the mechanical, tribological and structural properties of NiMo-(h)BN co-depositon produced by adding BN(h) to NiMo deposits optimized using different current coating techniques were analyzed and the tribological advantages offered by these coatings under high temperature conditions were evaluated and presented in the study.

2. General Methods

Two-dimensional boron nitride (BN(h)) nanosheets, intended for use as reinforcement elements within electrodeposited Ni-Mo alloy coatings, were synthesized via a metallothermic reduction process. Sodium tetraborate ($\text{Na}_2\text{B}_4\text{O}_7$) and metallic magnesium served as raw materials, while magnesium chloride (MgCl_2) was utilized to create the environment necessary for the reaction. Sodium tetraborate and metallic magnesium were mechanically mixed with magnesium chloride powder in stoichiometrically imbalanced ratios using a mortar.

The proportion of magnesium chloride to sodium tetraborate and metallic magnesium was set at 4:1. The resulting mixture was transferred to a crucible and placed in a tube furnace under a nitrogen atmosphere. The mixture was heated to 1200°C with the heating regime of $5^\circ\text{C}/\text{min}$ for 3 hours. After the magnesiothermic reduction reaction, two-dimensional BN(h) nanosheets were first reacted with sulfuric acid (2 M) for 12 hours to remove the Na, Mg oxide/chloride impurities and unreacted products formed as reaction products.

Stainless steels are used as a substrate for duplex NiP/NiMo alloy and duplex NiP/NiMo-(h)BN co-electrodeposition. To ensure a uniform surface before coating process, the stainless-steel substrates were cut to 4x4 cm dimensions, ground sequentially with SiC abrasive papers of from 120 to 1200 grit and polished with an

Al₂O₃-containing solution to prepare them for acidic pretreatment. Finally, the samples were etched by immersion in concentrated HCl solution for one minute.

NiP deposits were applied as the inner layer, and NiMo-(h)BN co-electrodeposition were applied as the outer layer. The coating bath components and operating conditions for the electrodeposition NiP (inner layer) are given in Table 1. Before NiMo-(h)BN co-electrodeposition optimization studies for NiMo

electrodeposition were conducted using various current modes, including direct current (DC), pulse current (PC), and pulse reverse current (PRC), to determine the optimal current type and conditions for composite coating. Ultrasound homogenization is applied to prevent agglomeration and improve the dispersion of (h)BN nanosheets in the NiMo deposition layer. The bath compositions for NiMo and NiMo-(h)BN co-electrodeposition are provided in Table 2.

Table 1. The coating bath components and operating conditions of NiP electrodeposition

Bath components		Operating Conditions	
Nickel Sulphate (NiSO ₄ .6H ₂ O)	180 g/L	Temperature	60±5 °C
Nickel Chloride (NiCl ₂ .6H ₂ O)	10 g/L	Current Density	2 A/dm ²
Trisodium citrate (C ₆ H ₅ O ₇ 3Na. 2H ₂ O)	70 g/L	pH	4-5
Phosphorous acid (H ₃ PO ₃)	20 g/L	Magnetic stirring	300 rpm
Phosphoric Acid (H ₃ PO ₄)	10 mL/L	Immersion time	15 min.
		Current type	PC
		Anode	Nickel

Table 2. The coating bath components and operating conditions of NiMo alloy and NiMo-(h)BN co-electrodeposition

	NiP/NiMo	Ni-P/Ni-Mo-(h)BN
Nickel Sulphate (NiSO ₄ .6H ₂ O)	197.2 g/L	197.2 g/L
Sodium Molybdate (Na ₂ MoO ₄ .2H ₂ O)	7.7 g/L	7.7 g/L
Trisodium citrate (C ₆ H ₅ O ₇ 3Na. 2H ₂ O)	132.3 g/L	132.3 g/L
Saccharin (C ₇ H ₅ NO ₃ S)	1 g/L	1 g/L
Sodium Lauryl Sulfate (SLS) (NaCH ₃ (CH ₂) ₁₁ OSO ₃)	62.5 mg/L	62.5 mg/L
Hexadecyltrimethylammonium bromide (CTAB (CH ₃ (CH ₂) ₁₅ N(Br)(CH ₃) ₃ BN(h))	-	62.5 mg/L
Temperature	Room temperature	Room temperature
pH	7	7
Immersion time	60 min.	60 min.
Magnetic stirrer	300 rpm	300 rpm
Current Type	DC, PC, PRC	PRC
Average current density	1 A/dm ²	1 A/dm ²
Anode	Nickel	Nickel

The morphologies and elemental compositions of the synthesized (h)BN nanosheets and coatings were analyzed using a scanning electron microscope (JEOL JSM-6060 LV) equipped with energy-dispersive spectrometry (EDS). Additionally, chemical composition and phase analyses of the samples were conducted using X-ray diffraction (XRD). The nano-hardness of the coatings was measured using nanoindentation (Anton Paar, Nano Indentation Tester-NHT3) on

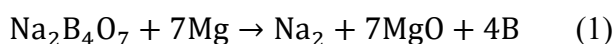
cross-sections, following the Oliver and Parr method [16].

Tribological tests were conducted at room temperature and at 400°C using the ball-on-disk method (Anton Paar, High Temperature Tribometer) to evaluate the coatings' operational stability under high-temperature conditions. Alumina balls with a diameter of 6 mm were used as counter material in tribological tests. The sliding speed was maintained at 10 cm/s.

Tribological tests were carried out under a 2N load over a sliding distance of 250 m. After tribological tests, wear tracks were examined by SEM. Additionally, the wear track topography is observed by using 3D profilometer (KLA Tencor P6).

3. Results and Discussion

Figures 1a and 1b present SEM images of the synthesized (h)BN nanosheets at different magnifications. The formation of the two-dimensional (h)BN nanosheets was achieved in four main steps: (i) boron formation via magnesiothermic reduction, (ii) generation of nanoscale boron nitride particles through boron nitridation, (iii) growth of nanoscale boron nitride particles along a specific plane, and (iv) grain coarsening through Ostwald ripening facilitated by a directed bonding mechanism [17]. The reactions involved in BN(h) nanosheet synthesis are shown in Equations (1) and (2):



At the synthesis temperature for BN(h) nanosheets, MgCl_2 (Tm: 714 °C) and $\text{Na}_2\text{B}_4\text{O}_7$ (Tm: 743 °C) interact to form a melt. In this melt, amorphous boron particles are produced through the reduction of molten $\text{Na}_2\text{B}_4\text{O}_7$ with metallic magnesium as indicated in Reaction (1). Given that magnesium has a vaporization point of 1090 °C, it exhibits a tendency to vaporize at 1200 °C without reacting. To prevent the vaporization of Mg, MgCl_2 , which melts at this temperature, is added in substantial amounts to function as a slag-forming agent and to reduce the vaporization tendency. During the reaction, the continuous flow of nitrogen gas supplied to the tube furnace promotes the formation of two-dimensional (h)BN nanosheets without the agglomeration of amorphous boron particles, as shown in Reaction (2) [18].

Figure 1c provides EDS analysis results for the BN(h) nanosheets. The EDS results reveal two prominent peaks corresponding to B and N, indicating that the majority of the (h)BN powder structure consists of (h)BN nanosheets. Figure 1d shows the XRD patterns of the (h)BN

nanosheets. Analysis of the XRD patterns identifies (h)BN at 2θ of 26.73°, 41.67°, 43.97°, and 55.29° (JCPDS no: 01-073-2095). Feng Liang et al. synthesized (h)BN nanosheets via the magnesiothermic reduction method, reporting the presence of hexagonal BN powder at 26.67°, 41.66°, and 55.16° in their XRD analysis [19]. In a similar study, Örnek et al. achieved the synthesis of hexagonal BN powder, with XRD results showing peaks at 2θ of 27.1°, 41.9°, 43.8°, 50.7°, and 55.4° for hexagonal BN powder [20].

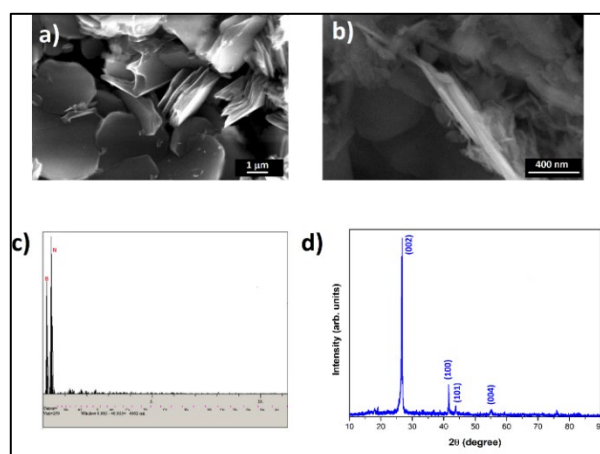


Figure 1. a) and b) The SEM image, c) EDS results and d) X-ray diffraction of (h)BN nano sheets

Figure 2a shows the surface and Figure 2b shows the cross-sectional images of the NiP alloy electrodeposition. From the surface and cross-sectional images, it is evident that the NiP alloy electrodeposition was successfully obtained.

Figure 2c presents the XRD patterns of the NiP alloy electrodeposition displaying a nickel peak at 2θ of 44.42° (JCPDS no: 01-070-1849). A homogeneous cross-sectional view was achieved using the pulsed current of the NiP alloy electrodeposition. Figures 2a and b clearly show the absence of discontinuities or cracks within the coating. Furthermore, the void-free, compact, and crack-free formation between the substrate-coating interface indicates a strong adhesion of the coating layer. The effect of the current type on the electrodeposition of NiMo outer layer.

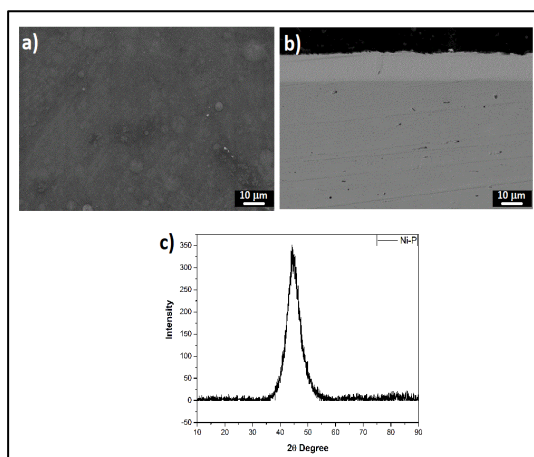


Figure 2. SEM images of a) surface, b) cross-sectional and c) XRD patterns of inner NiP layer

Figures 3a and 3b show the surface and cross-sectional images of electrodeposits produced with direct current (DC), Figures 3c and 3d with pulsed current (PC), and Figures 3e and 3f with reverse pulsed current (PRC). During the coating process, an average current density of 1 A/dm² was maintained constant to examine the effect of DC, PC, and PRC on the coating layer.

In the PRC method, the ton and toff times were kept constant to investigate the effect of the reverse current applied. In the DC-applied plating the growth morphology of the nickel-molybdenum alloy electrodeposition is dendritic and discontinuous. Figure 4c shows the molybdenum content by weight, obtained through EDS analysis of the coatings produced with different current types. The increased molybdenum content causes internal stress, leading to cracking in the coatings; hence, cracks are observed in the DC electrodeposition. Additionally, inhomogeneities are present within the coating layer.

To examine the nickel-molybdenum alloy electrodeposition produced by PC method, it is evident that more rough surface formations appear in the growth morphology of the coating layer, with an irregular surface structure; however, a crack-free structure is observed, likely due to the lower molybdenum content in the PC electrodeposition. In the nickel-molybdenum alloy electrodeposition produced with PRC, peak formations have disappeared, a homogeneous deposition is observed, and the structure contains significantly fewer cracks compared to electrodeposits produced by DC and

PC methods. In the PRC method, the application of reverse current (where the anode and cathode alternate at specific intervals) results in poorly adhered and unevenly deposited nickel ions returning to the solution, removing the peaks and creating a more homogeneous and smooth coating layer.

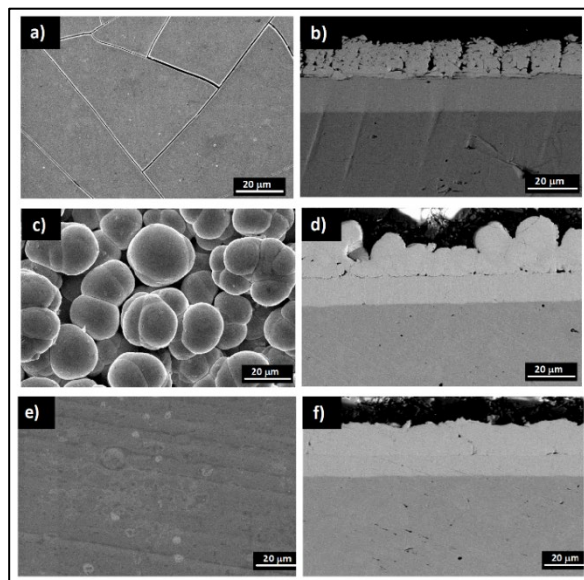


Figure 3. The surface morphology of duplex NiP/NiMo alloy electrodeposition fabricated by different current types of a-b) DC, c-d) PC and e-f) PRC

Chandrasekar et al. reported that the reverse pulsed current technique yields smoother coatings compared to those obtained by DC. They attributed this to the absence of pulsation in DC and the application of short anodic pulses during cathodic pulses in the PRC technique, which preferentially redissolves the dendritic structure formed during the cathodic pulses [1]. Furthermore, in this method, the coarse particles are reduced in size, allowing the subsequent grains to stack more evenly. This improves surface smoothness and reduces internal stress. Haseko et al. reported that coatings produced using the pulsed current (PC) method were superior to those obtained via direct current (DC) technique, and that the reverse pulsed current (PRC) method further improved the coating layer due to the periodic reversal of current direction [21]. Coatings produced using the PC method exhibited lower porosity compared to those achieved with the DC technique [22]. Additionally, they noted that by controlling the current and duration in both the PC and PRC

methods, finer crystal structures could be achieved [21].

The phase structures of duplex NiP/NiMo alloy electrodepositions produced by different current types were characterized using the XRD method. The resulting coatings, which do not contain any Mo-rich or NiMo-based intermetallic phases, exhibit a face-centered cubic NiMo solid solution structure. The effect of different current types on the XRD pattern is presented in Figure 4a. The peak at 2θ of 44.27° corresponds to nickel oriented in the typical (111) plane.

In the NiMo coatings, the peak at 2θ of 51.6° is associated with the (200) plane of nickel, while the peak at 2θ of 75.83° corresponds to nickel grown along the (220) plane (JCPDS no: 01-089-7128). Liu et al. reported that an increase in molybdenum content promotes the amorphization of the coating [23]. The peak observed at 2θ of 51.6° in the DC coating is broader and resembles an amorphous structure. Figure 4b displays the load-penetration depth curves for duplex NiP/NiMo alloy electrodepositions produced with various current types, while Figure 4c presents the corresponding hardness values. An examination of the hardness values shows that the coating produced by the DC method has a hardness of 5.32 GPa, the PC coating has a hardness of 2.676 GPa, and the PRC-produced duplex NiP/NiMo alloy electrodeposit has a hardness of 4.26 GPa.

The hardness values of the duplex NiP/NiMo alloy electrodeposits produced by different current types are consistent with their surface morphologies.

Due to the high molybdenum content, DC coatings are characterized by a brittle and hard nature. Among the coatings compared based on the applied current type, those produced by the PC method, which exhibit the lowest molybdenum content, have the lowest hardness values. Two-dimensional (h)BN nanosheets, produced via the metallothermic reduction method, were incorporated as reinforcement into the NiMo matrix in duplex NiP/NiMo co-electrodeposited. Figure 5a shows the surface image of the duplex NiP/NiMo-(h)BN co-electrodeposited coating.

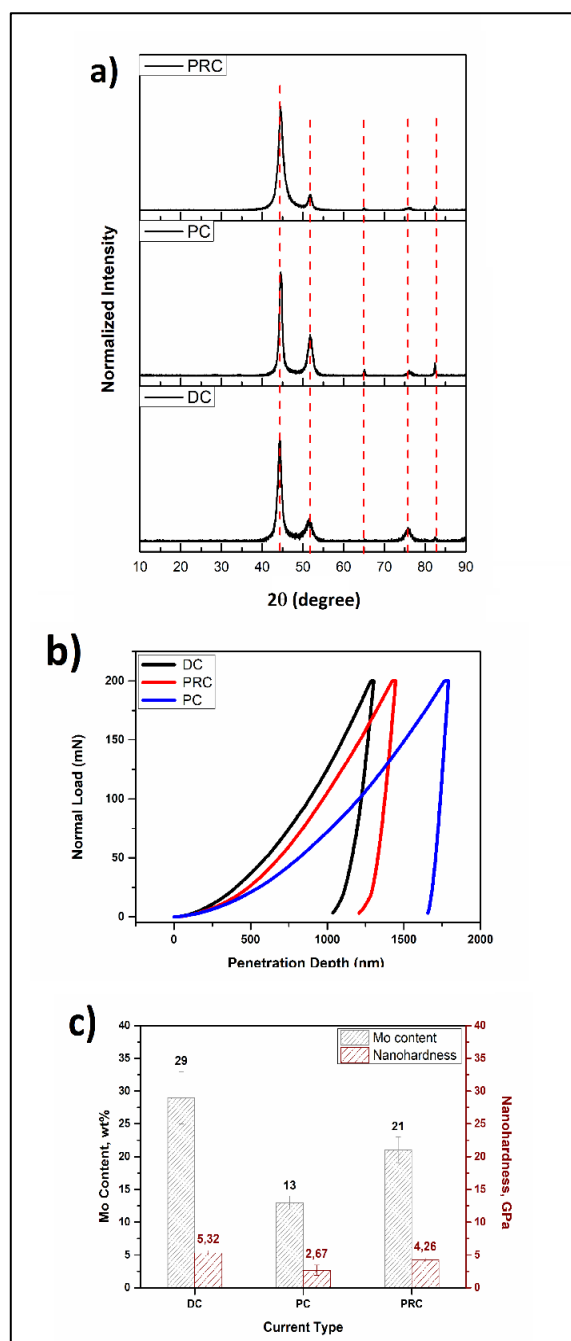


Figure 4. a) XRD patterns, b) nano indentation load vs. displacement curves, c) Mo content (wt.%) and nanohardness values (GPa) of duplex NiP/NiMo alloy electrodepositions produced by different current types of DC, PC and PRC

As seen in Figure 3e, the duplex NiMo alloy electrodeposits produced by the PRC method exhibit a smooth and dense surface structure. (h)BN, reinforced into the coating matrix, plays a significant role in altering the surface morphology. Additionally, due to the high Mo content in the plating capillary cracks have formed. It was previously noted that an increased molybdenum content can lead to cracking within the coating. The (h)BN nanosheets, incorporated

as reinforcement, prevent columnar growth and result in a rougher surface with spherical accumulations in duplex NiP/NiMo-(h)BN co-electrodeposits compared to duplex NiP/NiMo alloy electrodeposits. Dilek et al. reported that TiO₂, reinforced into a NiW matrix, increases surface roughness and creates a spherical growth morphology compared to alloy NiW coatings, attributing the cause of non-uniform grain growth to the preferential growth of nickel atoms on the nickel grains influenced by TiO₂ beneath them [24].

Figure 5b shows the cross-sectional view of the duplex NiP/NiMo-(h)BN co-electrodeposition. It demonstrates the successful deposition of the NiP alloy electrodeposit onto the substrate material. The NiMo-(h)BN layer, deposited onto the NiP alloy electrodeposition was successfully plated, forming a duplex NiP/NiMo-(h)BN structure. Examining Figure 5b, it is evident that the coating exhibits a rougher surface compared to Figure 2f. The presence of mounds and oval shapes, rather than smooth interfaces and outer surfaces, is attributed to the addition of (h)BN has a reinforcement material. Figure 5c displays the XRD patterns for duplex NiP/NiMo alloy electrodeposition and duplex NiP/NiMo-(h)BN co-electrodeposition. Upon examining Figure 5c, it is evident that the addition of (h)BN reinforcement leads to changes in the peaks and variations in crystal growth, particularly with a reduction in the intensity of the Ni (200) plane at 2 θ of 75.83°, suggesting an effect on crystal growth.

Figure 6 presents the load-penetration curves and shows the impact of (h)BN reinforcement on the hardness value of the duplex NiP/NiMo alloy and duplex NiP/NiMo-(h)BN co-electrodepositions. With the addition of (h)BN, the coating hardness increased from 4.26 GPa to 5.232 GPa, while the Mo content increased from 18 wt.% to 21 wt.%. This indicates that the weight percent of Mo in composite coatings increases with (h)BN reinforcement, suggesting that the presence of (h)BN nanosheets in the coating bath somewhat facilitates molybdenum accumulation.

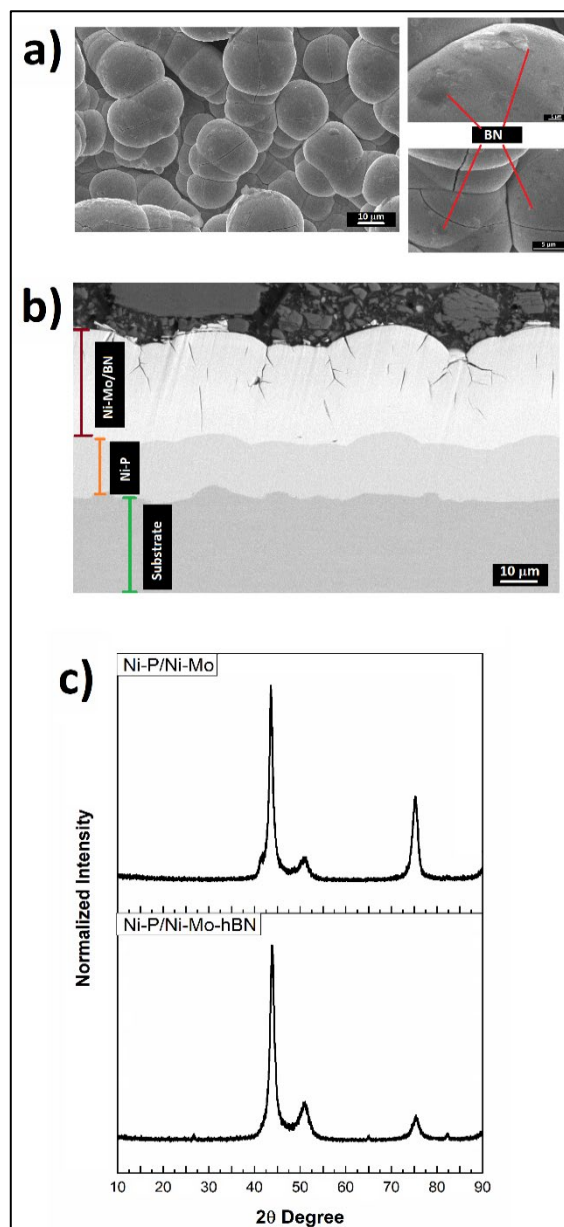


Figure 5. a) Surface morphology, b) cross sectional SEM images and c) XRD patterns of duplex NiP/NiMo-(h)BN co-electrodeposition

Laszczyńska et al. reported in their study that an increase in ZrO₂ in the solution of NiMo-ZrO₂ composite coatings correlates with an increase in Mo content, attributing this effect to the ZrO₂ particles facilitating the reduction of Mo [12].

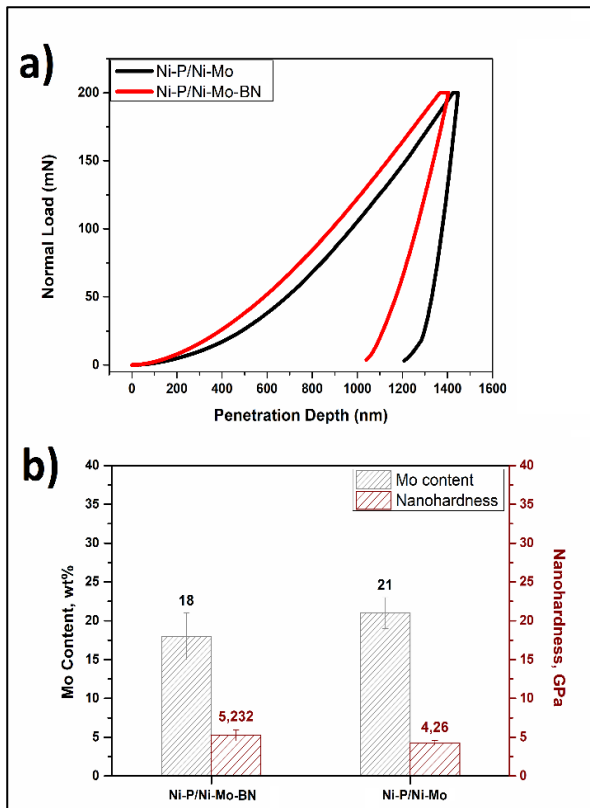


Figure 6. a) Nano indentation load vs. displacement curves, b) Mo content (wt.%) and nanohardness values (GPa) of duplex NiP/NiMo alloy and duplex NiP/NiMo-(h)BN co-electrodepositions

Figure 7 presents friction coefficient graphs for duplex NiP/NiMo alloy and duplex NiP/NiMo-(h)BN co-electrodepositions at room temperature and at 400°C. As observed in the friction coefficient curves in Figure 7a, the (h)BN reinforcement significantly reduces the coating's friction coefficient to approximately 0.4 μ . The wear rates indicate that sliding occurs within the layered lattice structure of the (h)BN particles, which is attributed to the hexagonal structure of (h)BN nanosheets [25]. Due to the non-stick nature of boron nitride particles, the likelihood of adhesion between the two contacting surfaces is reduced.

Figure 7b shows the comparative friction coefficient and wear rates for duplex NiP/NiMo alloy and duplex NiP/NiMo-(h)BN co-electrodepositions subjected to high-temperature wear at 400 °C. As can be seen, an increase in test temperature leads to a rise in the friction coefficient, due to the increased number of interactions between the asperities of the matching surfaces. This is because the contact area between matching surfaces increases exponentially with temperature [26, 27].

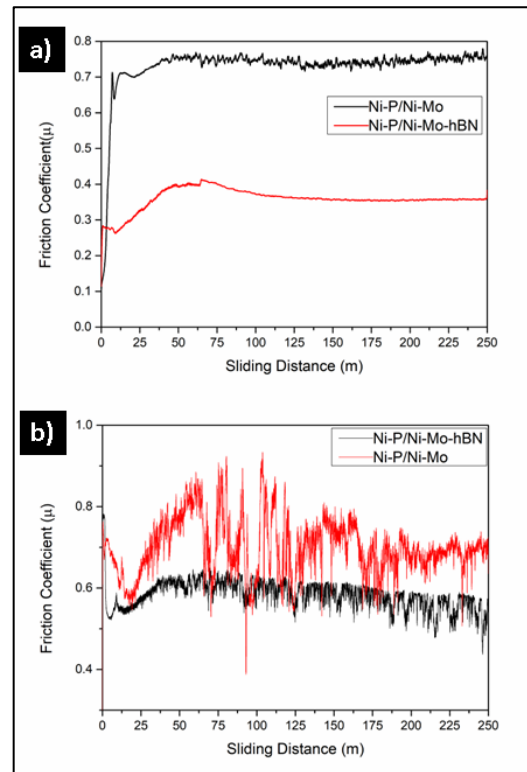


Figure 7. COF curves of duplex NiP/NiMo alloy and duplex NiP/NiMo-(h)BN co-electrodepositions at the a) room temperature and b) 400 °C

At high temperatures, these contacts may form very strong bonds, which subsequently break, often due to failure resulting from plastic flow and creep [26, 28, 29]. The obtained data align with the literature and are characteristic of typical nickel coatings. Comparing friction coefficients reveals that the (h)BN reinforcement reduces the friction coefficient even in the high-temperature wear test.

This result indicates that the (h)BN reinforcement retains its properties at elevated temperatures. The wear rate values also support the observed friction coefficients. With increasing temperature, an increase in adhesive wear components is noted due to the softening of the coatings. An increase in contact area between the abrasive ball and the coating surface is also observed. The shift in wear mechanism to more severe wear, characterized by plastic deformation and increased material transfer to the alumina counter face, is clearly evident in Figure 7.

The wear rate was determined using the following equation [30]:

$$\text{Wear rate} = \frac{V}{P \times S} \quad (3)$$

where: V represents the wear volume in mm^3 , P denotes the applied load in N , and S indicates the sliding distance. The wear rate of the duplex NiP/NiMo alloy electrodeposit at room temperature is calculated as $2.432 \times 10^{-5} \text{ mm}^3/\text{Nm}$, while at 400°C , the wear rate is $2.498 \times 10^{-5} \text{ mm}^3/\text{Nm}$. In contrast, the wear rates of the duplex NiP/NiMo-(h)BN co-electrodeposits are calculated as $1.723 \times 10^{-5} \text{ mm}^3/\text{Nm}$ at room temperature and $1.77 \times 10^{-5} \text{ mm}^3/\text{Nm}$ at 400°C . This indicates that the duplex NiP/NiMo-(h)BN co-electrodepositions are nearly twice as resistant to wear compared to duplex NiP/NiMo alloy electrodeposits, both at room temperature and at elevated temperatures. This improvement is attributed to the (h)BN reinforcement component, which provides a lubricating effect within the structure, thereby protecting it against wear.

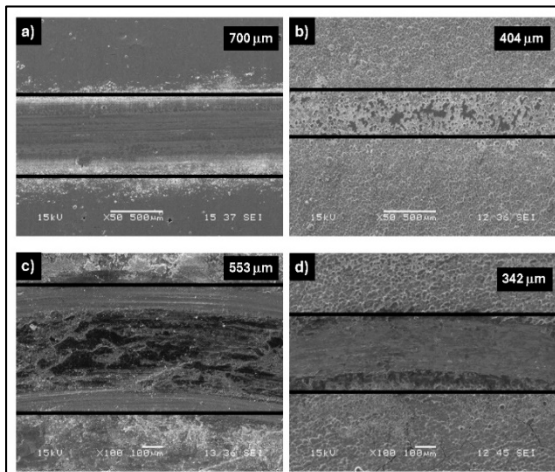


Figure 8. Low magnification SEM morphologies of the wear tracks of a) duplex NiP/NiMo alloy electrodeposits at the room temperature, b) at 400°C , c) duplex NiP/NiMo-(h)BN co-electrodeposits at the room temperature and d) 400°C

Figure 8 presents SEM images of the worn surfaces at low magnification, illustrating how (h)BN reinforcement affects the wear behavior of duplex NiP/NiMo alloy electrodeposits at room temperature and 400°C . At room temperature, the wear track width of duplex NiP/NiMo alloy electrodeposit is found as $700 \mu\text{m}$. With addition of (h)BN in the NiMo matrix, track width decreases, likely due to the increased hardness of the composite coatings and the role of (h)BN nanosheets as load-bearing and solid lubricating elements in the structure [31]. The effect of (h)BN at high temperatures becomes more evident with the reduction in wear track width.

The high-temperature resistance and self-lubricating properties of (h)BN show that it provides more effective protection against wear at 400°C

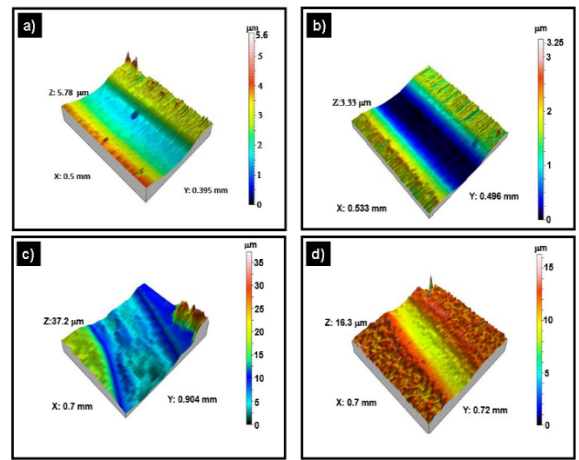


Figure 9. 3D profilometer results from wear tracks for a) duplex NiP/NiMo alloy coating, b) duplex NiP/NiMo-(h)BN co-electrodeposits tested at room temperature and c) duplex NiP/NiMo alloy, d) duplex NiP/NiMo-(h)BN co-electrodeposits tested at 400°C

Examining the 3D profilometer results of the wear tracks from room temperature wear tests for Ni-Mo coatings in Figure 9a, the characteristics of abrasive wear emerge with an approximate depth of $5.6 \mu\text{m}$. With reinforced h(BN) into the Ni-Mo matrix, it is evident from Figure 9b that the wear characteristics change, with the surface exhibiting more homogeneous wear and the wear depth reducing significantly to about $3.25 \mu\text{m}$. Figure 9c depicts the surface topography of Ni-Mo after wear tests at 400°C , while Figure 9d illustrates the corresponding topography for the Ni-Mo-(h)BN composite structure. It is observed that under high-temperature wear conditions, the Ni-Mo matrix is poorly preserved, with a wear depth reaching approximately $36 \mu\text{m}$. However, with the addition of h(BN) reinforcement to the Ni-Mo matrix, the wear depth is reduced to around $15 \mu\text{m}$. This enhancement is credited to the lubricating characteristics of h(BN), which bolster wear resistance under elevated temperatures.

As shown in Figures 10a and 10b, there is significant material loss and detachment, accompanied by small-scale tearing. The dominant mechanism observed is adhesive wear. It is evident that the smoothness of the wear

surfaces has improved with the addition of (h)BN reinforcement. Due to the lubricating properties provided by the hexagonal structure of (h)BN, material loss has been mitigated, or at least reduced to minimal levels, and no tearing has occurred. Furthermore, the (h)BN reinforcement has effectively decreased the contact area between the abrasive ball and the Ni-Mo base matrix.

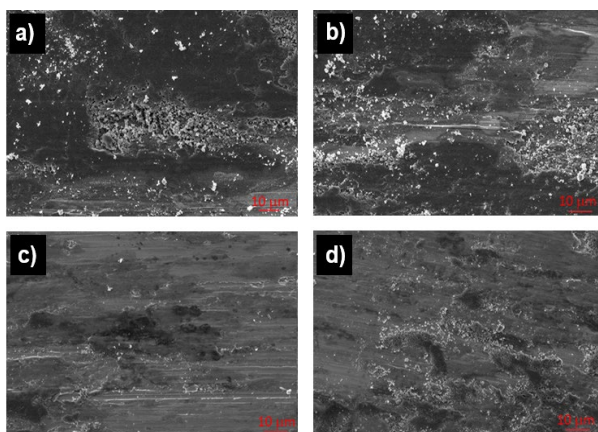


Figure 10. High magnifications SEM images from wear worms a) Ni-Mo at room temperature, b) Ni-Mo at 400°C, c) Ni-Mo-(h)BN at room temperature, d) Ni-Mo-(h)BN at 400°C

4. Conclusion

Two-dimensional (h)BN nanosheets were successfully synthesized using the metallothermic reduction method. The production of the NiP alloy electrodeposit the inner layer of the duplex plating was successfully achieved using the PC (pulsed current) method. In the production of the duplex NiMo alloy electrodeposit which forms the outer layer of the duplex structure, DC (direct current), PC, and PRC (reverse pulsed current) methods were tested, with characterization studies showing that PRC is the optimal current method. Two-dimensional (h)BN nanosheets were reinforced into the NiMo matrix of the outer layer of the duplex NiP/NiMo alloy electrodeposit and characterization studies examined the effects of this reinforcement on the matrix. Wear resistance tests at room temperature and at 400°C indicated that the addition of (h)BN significantly improved the wear resistance of duplex NiP/NiMo-(h)BN co-electrodepositions across high temperatures.

Article Information Form

Acknowledgments

We would like to thank Etimaden A.Ş. for providing us with the sodium tetraborate used in this study.

Funding

This work is supported by Sakarya University Science Research Projects Coordinators under contract number SAU BAP 2020-7-24-86. The authors thank the SAU BAP workers for their financial support.

Authors' Contribution

Authors contributed equally to the study.

The Declaration of Conflict of Interest/ Common Interest

No conflict of interest or common interest has been declared by authors.

The Declaration of Ethics Committee Approval

This study does not require ethics committee permission or any special permission.

The Declaration of Research and Publication Ethics

Authors of the paper declare that they comply with the scientific, ethical and quotation rules of SAUJS in all processes of the paper and that they do not make any falsification on the data collected. In addition, they declare that Sakarya University Journal of Science and its editorial board have no responsibility for any ethical violations that may be encountered, and that this study has not been evaluated in any academic publication environment other than Sakarya University Journal of Science.

Copyright Statement

Authors own the copyright of their work published in the journal and their work is published under the CC BY-NC 4.0 license.

References

- [1] M. S. Chandrasekar, M. Pushpavanam, "Pulse and pulse reverse plating- Conceptual, advantages and applications," *Electrochimica Acta*, vol. 53, pp. 3313–3322, 2008.

- [2] S. Tan, H. Algül, E. Kiliçaslan, A. Alp, H. Akbulut, M. Uysal, "The effect of ultrasonic power on high temperature wear and corrosion resistance for Ni based alloy composite coatings," *Colloids and Surfaces A: Physicochemical and Engineering Aspects*, vol. 656, pp.130345, 2023.
- [3] B. Pan, Y. Yao, L. Peng, Q. Zhang, Y. Yang, "Ultrasound-assisted pulse electrodeposition of cobalt films," *Materials Chemistry and Physics*, vol. 241, pp. 122395, 2020.
- [4] S. I. Ghazanlou, S. Ahmadiyah, R. Yavari, "Investigation of pulse electrodeposited Ni-Co/SiO₂ nanocomposite plating" *Surface Engineering*, vol. 33, pp. 337-347, 2017.
- [5] Y. Wang, L. Guan, Z. He, S. Zhang, H. Singh, M.D. Hayat, C. Yao, "Influence of pretreatments on physicochemical properties of Ni-P coatings electrodeposited on aluminum alloy," *Materials and Design*, vol. 197, pp. 109233, 2021.
- [6] A. A. Wronkowska, A. Wronkowski, "Optical properties of polycrystalline and amorphous Ni_{1-x}P_x layers by ellipsometry," *Journal of Materials Science* vol. 27, pp. 1842-1848, 1992.
- [7] F. E. T. Heakal, M. A. Shoeib, M. A. Maanoun, "Optimizing parameters affecting electroless Ni-P coatings on AZ91D magnesium alloy as corrosion protection barriers," *Protection of Metals and Physical Chemistry of Surfaces*, vol. 53, pp. 177-187, 2017.
- [8] E. W. Brooman, "Corrosion behavior of environmentally acceptable alternatives to cadmium and chromium coatings: Cadmium. Part I," *Metal Finishing*, vol. 98, pp.42-50, 2000.
- [9] V. Torabinejad, M. Aliofkhaezai, A.S. Rouhaghdam, M. H. Allahyarzadeh, "Electrodeposition of Ni-Fe-Mn/Al₂O₃ functionally graded nanocomposite coatings," *Surface Engineering*, vol. 33, pp.122-130,2017.
- [10] P. Kedzierzawski, D. Oleszak, M. Janik-Czachor, "Hydrogen evolution on hot and cold consolidated Ni-Mo alloys produced by mechanical alloying," *Materials Science and Engineering: A*, vol. 300, pp. 105-112, 2001.
- [11] E. Ünal, H. Karahan, "Production and characterization of electrodeposited Ni-B/hBN composite coatings", *Surface and Coatings Technology*, vol. 333, pp.125-137, 2018.
- [12] A. Laszczyńska, J. Winiarski, B. Szczygieł, I. Szczygieł, "Electrodeposition and characterization of Ni-Mo-ZrO₂ composite coatings," *Applied Surface Science*, vol. 369, pp. 224-231,2016.
- [13] Y. Xu, B. Liang, Y. Gao, J. Zou, R. Hua, Y. Z. Sun, Y. Chen, Q. Zhao, "Pulse electrodeposition of a duplex-layer structured composite nickel-based coating with improved corrosion and abrasion resistance," *Ceramic International*, vol. 50, pp. 10515-10524, 2024.
- [14] B. Li, W. Zhang, D. Li, Y. Huan, J. Dong, "Microstructural, surface and electrochemical properties of a novel Ni-B/Ni-W-BN duplex composite coating by co-electrodeposition," *Applied Surface Science*, vol. 458, pp. 305-318, 2018.
- [15] M. S. Safavi, A. Rasooli, F. A. Sorkhabi, "Electrodeposition of Ni-P/Ni-Co-Al₂O₃ duplex nanocomposite coatings: towards improved mechanical and corrosion properties," *Transactions of the Institute of Metal Finishing*, vol. 98, pp. 320-327, 2020.
- [16] H. Algul, M. Uysal, A. Alp, "A comparative study on morphological, mechanical and tribological properties of electroless NiP, NiB and NiBP coatings," *Applied Surface Science Advances*, vol. 4, pp. 100089, 2021.

- [17] K. Bao, F. Yu, L. Shi, S. Liu, X. Hu, J. Cao, Y. Qian, "Synthesis of highly crystalline rhombohedral BN triangular nanoplates via a convenient solid state reaction," *Journal of Solid State Chemistry*, vol. 182, pp.925-931, 2009.
- [18] L. Ye, L. Zhao, F. Liang, X. He, W. Fang, H. Chen, S. Zhang, S. An, "Facile synthesis of hexagonal boron nitride nanoplates via molten-salt-mediated magnesiothermic reduction," *Ceramic International*, vol. 41, pp. 14941–14948, 2015.
- [19] Q. Li, C. Lee, R. W. Carpick, J. Hone, "Substrate effect on thickness-dependent friction on graphene," *Physica Status Solidi (B) – Basic Solid State Physics*, vol. 247, pp. 2909-2914, 2010.
- [20] M. Örneke, K. Wang, S. Xiang, C. Hwang, K. Y. Xie, R. A. Haber, "Molten salt synthesis of highly ordered and nanostructured hexagonal boron nitride," *Diamond and Related Materials*, vol. 93, pp. 179–186, 2019.
- [21] Y. Haseko, N. K. Shrestha, S. Teruyama, T. Saji, "Reversal pulsing electrodeposition of Ni/polypyrrole composite film," *Electrochimica Acta*, vol. 51, pp. 3652–3657, 2006.
- [22] C. Guo, Y. Zuo, X. Zhao, J. Zhao, J. Xiong, "The effects of pulse-reverse parameters on the properties of Ni-carbon nanotubes composite coatings," *Surface and Coating Technology*, vol. 201, pp. 9491-9496, 2007.
- [23] J. H. Liu, J. X. Yan, Z. L. Pei, J. Gong, C. Sun, "Effects of Mo content on the grain size, hardness and anti-wear performance of electrodeposited nanocrystalline and amorphous Ni–Mo alloys," *Surface and Coating Technology*, vol. 404, pp. 126476, 2020.
- [24] S. Dilek, H. Algül, A. Akyol, A. Alp, H. Akbulut, M. Uysal, "Pulse electro co-deposition of submicron-sized TiC reinforced Ni–W coatings: tribological and corrosion properties," *Journal of Asian Ceramic Societies*, vol. 9, pp. 673–685, 2021.
- [25] C. Baldwin, T. E. Such, "The Plating Rates and Physical Properties of Electroless Nickel/Phosphorus Alloy Deposits," *Transactions of the IMF*, vol. 46, pp. 73-80, 1968.
- [26] O. A. León, M. H. Staia, H. E. Hintermann, "Wear mechanism of Ni-P-BN(h) composite autocatalytic coatings," *Surface and Coating Technology*, vol. 200, pp. 1825-1829, 2005.
- [27] M. H. Staia, H. E. Hintermann, O. A. Leon, "Influence of the heat treatment on the tribological behavior of a Ni – P – BN (h) autocatalytic composite plating" *Surface and Coating Technology*, vol. 121, pp. 641-645, 1999.
- [28] F. Kiliç, H. Gül, S. Aslan, A. Alp, H. Akbulut, "Effect of CTAB concentration in the electrolyte on the tribological properties of nanoparticle SiC reinforced Ni metal matrix composite (MMC) coatings produced by electrodeposition," *Colloids and Surfaces A: Physicochemical and Engineering Aspects*, vol. 419, pp. 53-60, 2013.
- [29] H. Algul, H. Gul, M. Uysal, A. Alp, H. Akbulut, "Tribological Properties of TiO₂ Reinforced Nickel Based MMCs Produced by Pulse Electrodeposition Technique," *Transactions of the Indian Institute of Metals*, vol. 68, pp.79-87, 2014.
- [30] H. Akbulut, G. Hatipoglu, H. Algul, M. Tokur, M. Kartal, M. Uysal, T. Cetinkaya, "Co-deposition of Cu/WC/graphene hybrid nanocomposites produced by electrophoretic deposition," *Surface and Coating Technology*, vol. 284, pp. 344-352, 2015.
- [31] O. A. León, M. H. Staia, H. E. Hintermann, "High temperature wear of an electroless Ni-P-BN (h) composite plating" *Surface and Coating Technology*, vol. 163–164, pp. 578-584, 2003.